THE ASTROPHYSICAL JOURNAL, 537:205–220, 2000 July 1

STELLAR IRON ABUNDANCES AT THE GALACTIC CENTER

SOLANGE V. RAMÍREZ[1,2] AND K. SELLGREN[1,2]
Department of Astronomy, The Ohio State University, 140 West 18th Avenue, Columbus, OH 43210
JOHN S. CARR[2]
Naval Research Laboratory, Remote Sensing Division, Code 7217, Washington, DC 20375
SUCHITRA C. BALACHANDRAN[2]
Department of Astronomy, University of Maryland, College Park, MD 20742
ROBERT BLUM[1,2]
Cerro Tololo Inter-American Observatory, Casillo 603, La Serena, Chile
AND
DONALD M. TERNDRUP AND ADAM STEED
Department of Astronomy, The Ohio State University, 140 West 18th Avenue, Columbus, OH 43210
Received 1999 November 12; accepted 2000 February 1

ABSTRACT

We present measurements of [Fe/H] for six M supergiant stars and three giant stars within 2.5 pc of the Galactic center (GC) and one M supergiant star within 30 pc of the GC. The results are based on high-resolution ($\lambda/\Delta\lambda = 40{,}000$) K-band spectra, taken with CSHELL at the NASA Infrared Telescope Facility. We determine the iron abundance by detailed abundance analysis, performed with the spectral synthesis program MOOG. The mean [Fe/H] of the GC stars is determined to be near solar, [Fe/H] = $+0.12 \pm 0.22$. Our analysis is a *differential* analysis, as we have observed and applied the same analysis technique to 11 cool, luminous stars in the solar neighborhood with similar temperatures and luminosities as the GC stars. The mean [Fe/H] of the solar neighborhood comparison stars, [Fe/H] = $+0.03 \pm 0.16$, is similar to that of the GC stars. The width of the GC [Fe/H] distribution is found to be narrower than the width of the [Fe/H] distribution of Baade's window in the bulge but consistent with the width of the [Fe/H] distribution of giant and supergiant stars in the solar neighborhood.

Subject headings: Galaxy: abundances — Galaxy: center — Galaxy: stellar content — stars: abundances — stars: late-type

1. INTRODUCTION

Morris & Serabyn (1996) and Serabyn & Morris (1996) have summarized the relative importance of star formation, gas inflow, and gas outflow in the Galactic center (GC). Gas from the inner disk flows into the nucleus, perhaps driven by a bar potential (Stark et al. 1991; Morris & Serabyn 1996), and some of the stellar mass loss from the bulge may fall into the GC (Blitz et al. 1993; Jenkins & Binney 1994). Serabyn & Morris (1996) have proposed that this inflow of disk gas results in sustained star formation in a "central molecular zone" (CMZ) within a radius from the GC of $R \leq 200$ pc. The GC is observed to be currently forming stars in the CMZ at a rate of 0.3–0.6 $M_\odot$ yr^{-1} (Güsten 1989). Some of the GC gas incorporated into stars, enriched by stellar nucleosynthesis, will be returned to the GC interstellar medium by stellar mass loss and supernovae. X-ray observations of hot gas in the GC suggest that some gas could be driven temporarily or permanently from the GC by a galactic fountain or wind (Blitz et al. 1993; Morris & Serabyn 1996), however, making it unclear how much enriched material is incorporated into following generations of star formation. The presence of strong magnetic fields in the GC also likely plays a role in whether enriched gas is driven from or is retained within the GC.

Continued star formation in the central few hundred parsecs of the Galaxy may lead to higher metallicities within the CMZ. Chemical abundances in the disks of spiral galaxies are observed to reach their highest values at the center (see Pagel & Edmunds 1981; Shields 1990). H II regions, planetary nebulae, and OB associations in the Milky Way also show a radial metallicity gradient (Shaver et al. 1983; Fich & Silkey 1991; Maciel & Köppen 1994; Simpson et al. 1995; Vílchez & Esteban 1996; Rudolph et al. 1997; Afflerbach, Churchwell, & Werner 1997; Smartt & Rolleston 1997; Gummersbach et al. 1998). Chemical evolution models strive to explain these gradients by considering the relative star formation and gas infall/outflow rates, and the metal abundance of the gas compared to the stars (see Audouze & Tinsley 1976; Rana 1991).

The metallicity of GC stars is needed in order to constrain models and understand the stellar processes in the central parsecs of our Galaxy. Measurements of stellar metallicities in the center of the Milky Way, which is obscured by approximately 30 mag of extinction at V, are only now beginning to be feasible through infrared studies. Carr, Sellgren, & Balachandran (2000) found a solar Fe abundance in IRS 7, an M supergiant at a distance of $R = 0.2$ pc from the GC, from a detailed abundance analysis of CSHELL ($\lambda/\Delta\lambda = 40{,}000$) K-band spectra. Our work analyzes similar data for several M supergiant and giant stars located in the central cluster, within 2.5 pc of the

[1] Visiting Astronomer, Cerro Tololo Inter-American Observatory. CTIO is operated by AURA, Inc. under contract to the National Science Foundation.
[2] Visiting Astronomer, Infrared Telescope Facility. IRTF is operated by the University of Hawaii under contract to the National Aeronautics and Space Administration.

Report Documentation Page

Form Approved
OMB No. 0704-0188

1. REPORT DATE	2. REPORT TYPE	3. DATES COVERED
2000		**00-00-2000 to 00-00-2000**

4. TITLE AND SUBTITLE	5a. CONTRACT NUMBER
Stellar Iron Abundances at the Galactic Center	5b. GRANT NUMBER
	5c. PROGRAM ELEMENT NUMBER
6. AUTHOR(S)	5d. PROJECT NUMBER
	5e. TASK NUMBER
	5f. WORK UNIT NUMBER
7. PERFORMING ORGANIZATION NAME(S) AND ADDRESS(ES) **Naval Research Laboratory,Code 7217,4555 Overlook Avenue, SW,Washington,DC,20375**	8. PERFORMING ORGANIZATION REPORT NUMBER
9. SPONSORING/MONITORING AGENCY NAME(S) AND ADDRESS(ES)	10. SPONSOR/MONITOR'S ACRONYM(S)
	11. SPONSOR/MONITOR'S REPORT NUMBER(S)

12. DISTRIBUTION/AVAILABILITY STATEMENT
Approved for public release; distribution unlimited

13. SUPPLEMENTARY NOTES

14. ABSTRACT

15. SUBJECT TERMS

16. SECURITY CLASSIFICATION OF:			17. LIMITATION OF ABSTRACT	18. NUMBER OF PAGES	19a. NAME OF RESPONSIBLE PERSON
a. REPORT **unclassified**	b. ABSTRACT **unclassified**	c. THIS PAGE **unclassified**		**16**	

GC, and also one M supergiant star located in the Quintuplet cluster, 30 pc away from the GC.

2. OBSERVATIONS

2.1. *Sample Selection*

The GC stars were selected with three requirements. First, they have to be brighter than $K = 9.5$, a limit set by the sensitivity of the instrument. An hour of integration time is required for high signal-to-noise (S/N) spectra for a $K = 9$ star when observing with CSHELL at the NASA Infrared Telescope Facility (IRTF). Second, the stars should be cool luminous stars in order to ensure we are observing photospheric absorption lines rather than the stellar wind emission lines characteristic of hot luminous stars in the GC. Third, these cool luminous stars should have little or no water absorption. This is because published line lists for water (wavelengths, excitation potentials, dissociation potentials, oscillator strengths, and damping constants) are not yet adequate for detailed abundance analysis of high-resolution stellar spectra. The amount of water absorption is determined from *H*- and *K*-band low-resolution spectra ($\lambda/\Delta\lambda \sim 500$) taken with the IRS at CTIO (S. V. Ramírez, R. D. Blum, & K. Sellgren 2000, in preparation). The selected sample consists of nine stars located in the central cluster ($R < 2.5$ pc), and one star located in the Quintuplet cluster ($R = 30$ pc). The central cluster stars are IRS 7, IRS 11, IRS 19, IRS 22, BSD 72, BSD 114, BSD 124, BSD 129, and BSD 140 (names and positions are given by Blum, Sellgren, & DePoy 1996a). The star located in the Quintuplet cluster is VR 5-7 (Moneti, Glass, & Moorwood 1994). Eleven cool, luminous stars in the solar neighborhood were selected from the literature to be observed and analyzed the same way as the GC stars. These 11 stars have known abundances from detailed analysis in the optical (Luck 1982a, 1982b; Lambert et al. 1984; Smith & Lambert 1985, 1986; Luck & Bond 1989) and in the infrared (Carr et al. 2000). These cool, luminous stars in the solar neighborhood were carefully selected to be in the same range of effective temperature and surface gravity as the GC stars. This is very important in order to allow a differential analysis comparison, which will cancel possible systematic errors such as NLTE effects (see § 3.4). The selected cool, luminous stars in the solar neighborhood are listed in Table 1.

2.2. *Data Acquisition and Reduction*

The *K*-band high-resolution ($\lambda/\Delta\lambda = 40{,}000$) spectra used in the abundance analysis were taken with CSHELL at the IRTF. The IRTF is a 3 m telescope located at Mauna Kea Observatory in Hawaii, and CSHELL is the facility cryogenic infrared echelle spectrograph (Tokunaga et al. 1990). The observations were carried out in 1993 May, 1996 June, 1996 August, 1997 July, 1998 May, 1998 July, and 1999 June. The detector for the 1993 observations was a 256×256 NICMOS-3 HgCdTe array, which provided a spectral coverage of ≈ 1000 km s^{-1} or 73 Å. The detector for the rest of the observations was a 256×256 SBRC InSb array, which gives a smaller coverage of ≈ 750 km s^{-1} or 55 Å. The slit used to achieve a resolution of $\lambda/\Delta\lambda = 40{,}000$ is 0.5″ wide, 30″ long, with a pixel scale of 0.25″ pixel^{-1} for 1993 data and 0.20″ pixel^{-1} for later data. Our highest quality data were taken in 1998 and in 1999 when new order-separating circular variable filters were installed, providing spectra free of fringes.

Eight iron lines were selected by inspecting the high-resolution atlas of cool stars (Wallace & Hinkle 1996) and by analyzing synthetic spectra, which includes atomic and molecular features (see details in § 3 and in Carr et al. 2000). Thousands of lines of molecules such as CN, CO and H_2O are present throughout the infrared spectrum of cool stars. The selected iron lines are almost free of known molecular contamination and unidentified lines. The eight iron lines are observed using three grating settings of CSHELL. Atomic parameters of the eight iron lines used in the abundance analysis are listed in Table 2.

TABLE 1

STELLAR PARAMETERS FOR NEARBY LATE-TYPE STARS

Star	Spectral Type	S/N[a]	$T_{\rm eff}$[a] (K)	$M_{\rm bol}$[a]	log g[a]	ξ[a] (km s^{-1})	ζ[a] (km s^{-1})
HR 6146	M6 III[b]	45[c]	3250 ± 100[b]	-5.5[b]	0.2 ± 0.3[b]	2.0 ± 0.5[c]	9.6 ± 1.1[c]
HR 6702	M5 II–III[b]	36[c]	3300 ± 100[b]	-3.4[b]	0.7 ± 0.3[b]	2.0 ± 0.5[c]	7.8 ± 1.8[c]
HR 7442	M5 IIIas[d]	36[c]	3450 ± 100[d]	-4.0[d]	0.5 ± 0.3[d]	2.4 ± 0.2[c]	10.5 ± 2.7[c]
HR 8062	M4 IIIas[d]	34[c]	3450 ± 100[d]	-3.5[d]	0.7 ± 0.3[d]	1.7 ± 0.2[c]	8.9 ± 0.5[c]
α Ori	M1–2 Iab–a[e]	305[f]	3540 ± 260[e]	-7.4[g]	0.0 ± 0.3[g]	2.8 ± 0.2[c]	14.7 ± 0.5[c]
HR 8383	M2 Iape+[h]	100[c]	3480 ± 250[e]	-6.8[h,i]	0.0 ± 0.3[h]	2.7 ± 0.2[c]	14.4 ± 2.1[c]
HD 202380.....	M3 Ib[h]	46[c]	3600 ± 200[h]	-5.7[h,i]	0.6 ± 0.5[h]	2.5 ± 0.2[c]	16.2 ± 0.5[c]
HD 163428.....	K5 II[h]	67[c]	3800 ± 200[h]	-5.5[h,i]	0.6 ± 0.5[h]	2.3 ± 0.2[c]	11.5 ± 3.2[c]
BD +59°594.....	M1 Ib[j]	49[c]	4000 ± 200[j]	-6.6[i]	-0.9 ± 0.3[j]	3.1 ± 0.2[c]	18.2 ± 1.0[c]
HD 232766.....	M1 Iab[j]	38[c]	4000 ± 200[j]	-6.6[i]	0.2 ± 0.3[j]	2.2 ± 0.2[c]	11.5 ± 3.7[c]
HR 8726	K5 Iab[k]	57[c]	4000 ± 200[k]	-5.2[k,i]	0.5 ± 0.3[k]	2.4 ± 0.2[c]	11.4 ± 0.5[c]

[a] S/N = mean signal-to-noise ratio per pixel; $T_{\rm eff}$ = effective temperature; $M_{\rm bol}$ = bolometric magnitude; g = surface gravity; ξ = microturbulent velocity; ζ = macroturbulent velocity.
[b] Smith & Lambert 1985.
[c] This paper.
[d] Smith & Lambert 1986.
[e] Carr et al. 2000.
[f] Wallace & Hinkle 1996.
[g] Lambert et al. 1984.
[h] Luck 1982b.
[i] Lang 1991, p. 142.
[j] Luck & Bond 1989.
[k] Luck 1982a.

TABLE 2

Fe Line Data

Wavelength (Å)	χ (eV)[a]	log gf[a]
21781.82.....	3.415	−4.485
22381.27.....	5.844	−1.458
22386.90.....	5.033	−0.481
22391.22.....	5.320	−1.600
22398.98.....	5.099	−1.249
22818.82.....	5.792	−1.296
22838.60.....	5.099	−1.325
22852.17.....	5.828	−0.612

[a] χ = excitation potential; gf = gf-value determined in this paper.

Spectra were acquired at two different positions along the slit and reduced separately in order to determine any systematic effects such as fringes. Several individual spectrum pairs were observed per star, until the desired signal-to-noise ratio was reached. Stars of spectral type A or B were observed as close to the program star's air mass as possible in order to correct for telluric absorption features and to remove fringes. Such stars have no significant spectral features in the observed wavelength regions.

Image Reduction and Analysis Facility (IRAF[3]) and VISTA were used for data reduction. The reduction process began by flat-fielding the individual spectra with calibration lamp flats, which were taken for every grating setting. Sky subtraction was performed by subtracting two consecutive spectra taken at different positions along the slit. Bad pixels were replaced by an interpolated value computed from neighboring pixels in both the dispersion and perpendicular directions. Individual spectra were extracted with a 5 pixel wide aperture using the APSUM package in IRAF. Extracted spectra observed at the same position along the slit were averaged to produce two spectra per star, one spectrum for each position along the slit. Spectra of the program stars were then divided by the appropriate A- or B-type atmospheric standards, observed at the same position along the slit and reduced in the same way, to remove telluric absorption features and fringes. Each spectrum was then multiplied by a blackbody of the same temperature as the A or B star to put the spectra on a relative flux density (F_λ) scale. The temperature of the A or B star was determined from its spectral type. More than five telluric absorption lines were used to obtain wavelength solutions. The wavelength calibration was performed using the tasks of VISTA. Spectra were shifted in wavelength to correct for radial velocity differences, by comparing the observed and synthetic spectra. The spectra were normalized by a linear fit of continuum bands. These continuum bands were chosen by comparing the observed spectrum of α Ori from the high-resolution atlas (Wallace & Hinkle 1996) with the synthetic spectrum of α Ori. The bands selected are regions in the spectrum in which the synthesis and the normalized observations of α Ori are coincident and equal to unity. We estimated the error per pixel as the difference of observations taken at two positions along the slit. We computed the mean signal-to-noise ratio (S/N) per pixel by the average of the signal-to-noise ratio per pixel for all spectra observed for that star. The mean S/N per pixel for each star is listed in Tables 1 and 3.

[3] The IRAF software is distributed by the National Optical Astronomy Observatories under contract with the National Science Foundation.

3. ABUNDANCE ANALYSIS

The abundance analysis was done using a current version of the LTE spectral synthesis program MOOG (Sneden 1973). The program requires a line list giving the wavelength, excitation potential, gf-values, and damping constants for all atomic and molecular lines that contribute to the spectrum. The method used to construct the line list is described in § 3.1. In addition, an input model atmosphere for the effective temperature and surface gravity appropriate for each star and a value for the microturbulent velocity is also required. The solar abundance model atmospheres from Plez (Plez 1992; Plez, Brett, & Nordlund 1992) were used in our analysis because they are the only ones that include gravities and temperatures as low as those of the Galactic center stars. The Plez models also include sphericity, which is appropriate for supergiant stars (Plez et al. 1992). MOOG, however, does not account for sphericity in its calculations. Carr et al. (2000), who also used MOOG, compute the effective temperature and microturbulent velocity of α Ori, VV Cep (HR 8383), and β And using different sets of model atmospheres, including the Plez models and two plane-parallel atmospheres. When the

TABLE 3

Stellar Parameters for Galactic Center Stars

Star	Luminosity Class	S/N[a]	$T_{\rm eff}$[a] (K)	$M_{\rm bol}$[a,b]	M[a] ($M_\odot$)	log g[a]	ξ[a] (km s^{-1})	ζ[a] (km s^{-1})
IRS 7[c]	I	52	3470±250	−9.0	17±3	−0.6±0.2	3.3±0.4	20.6±2.7
VR 5-7.....	I	30	3500±300	−7.8	14±2	−0.2±0.3	2.9±0.5	12.6±1.6
IRS 19	I	75	3650±300	−7.2	14±2	0.1±0.3	2.7±0.5	13.4±2.0
IRS 22	I	25	3550±300	−6.4	10±2	0.3±0.3	2.5±0.5	12.8±1.6
BSD 124.....	I	10	3600±300	−5.5	7±3	0.4±0.3	2.4±0.5	12.7±2.7
BSD 129.....	I	13	3650±300	−5.3	7±3	0.5±0.3	2.4±0.5	12.3±2.7
BSD 72	I	13	3750±300	−4.5	5±2	0.8±0.3	2.1±0.5	11.0±2.7
BSD 114.....	III	15	3100±280	−5.8	3±1	−0.2±0.5	2.9±0.6	9.0±3.0
IRS 11	III	16	3100±280	−5.3	3±1	0.0±0.5	2.8±0.6	9.1±2.2
BSD 140.....	III	13	3100±280	−4.8	2.5±1	−0.1±0.5	2.9±0.6	9.0±3.0

[a] S/N = mean signal-to-noise ratio per pixel; $T_{\rm eff}$ = effective temperature; $M_{\rm bol}$ = bolometric magnitude; M = mass; g = surface gravity; ξ = microturbulent velocity; ζ = macroturbulent velocity.

[b] Error in $M_{\rm bol}$ is ±0.4 (Carr et al. 2000), dominated by the uncertainty in the extinction curve [$E(H-K)/A_K$].

[c] Stellar parameters from Carr et al. 2000.

stellar parameters derived from each model were used self-consistently to derive [Fe/H], the result for [Fe/H] was the same. The determination of the stellar parameters for our sample is discussed in § 3.2.

3.1. *Atomic and Molecular Parameters*

The line list was created the same way as that of Carr et al. (2000), using two main steps: (1) The solar spectrum was used to determine the *gf*-values and the damping constants, and (2) minor adjustments were made by comparison to the Arcturus spectrum (Wallace & Hinkle 1996). An initial line list was compiled using Fe I line positions and energy levels from Nave et al. (1994) and the Kurucz (1993) line lists for CN and other atomic lines. The damping constants for all atomic lines were initially set to twice that of the Unsöld approximation for van der Waals broadening (Holweger et al. 1991). A synthetic spectrum was generated for the Sun, using the Kurucz (1993) solar model. The *gf*-values and damping constants were adjusted to match the observed solar spectrum (Livingstone & Wallace 1991), when needed, and unidentified lines were noted. Then, a synthetic spectrum was generated for Arcturus, using the model atmosphere, stellar parameters, and abundances from Peterson, Dalle Ore, & Kurucz (1993). The solar line list provided a good match to the Arcturus spectrum. The *gf*-values of low-excitation lines, not observable in the Sun, had to be adjusted. The final Fe I atomic parameters are listed in Table 2. A synthetic spectrum of α Ori, generated using the final line list, is compared in Figure 1 to the observed spectrum from Wallace & Hinkle (1996) in the region of each of our eight Fe I lines. A Plez model atmosphere with the stellar parameters listed in Table 3, and the CNO abundances from Lambert et al. (1984) were used.

The depth of line formation was examined using contribution functions, which provide an indication of spectral line formation coming from different layers of a stellar model atmosphere (see details in Edmonds 1969; Sneden 1973). The determination of the depth of line formation is needed to make sure each line is formed in the range of opacity (τ) covered by our model atmosphere. The eight iron lines used in this abundance analysis are formed in the range of $-2.0 < \log \tau < 0.3$, where Plez model atmospheres cover a range of $-5.6 < \log \tau < 2.6$. Note that the Sc I lines in supergiant stars, which neither we nor Carr et al. (2000), who included hyperfine splitting calculations for Sc I lines, are able to model correctly, are shown by the contribution function to be partially formed at optical depths outside the range of the Plez models. We therefore approximately model Sc I lines by scaling the Fe I line profiles to the correct depth and width to allow us to separate the one Fe I line at 22399 Å that is blended with a Sc I line at 22400 Å. In the case of IRS 7 this procedure was not successful.

3.2. *Stellar Parameters*

3.2.1. *Effective Temperature*

The effective temperature ($T_{\rm eff}$) is a key parameter for any abundance analysis. For the cool, luminous stars in the solar neighborhood, the effective temperatures were taken

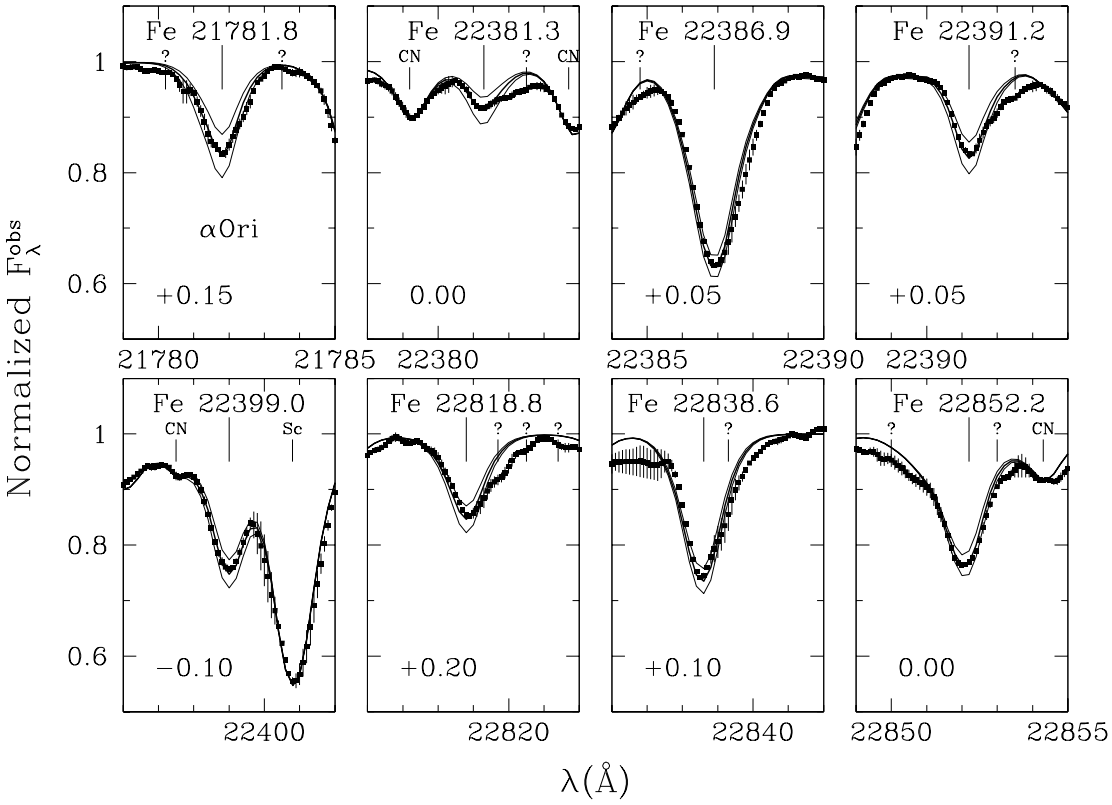

FIG. 1.—Observed spectrum (*filled squares*) of α Ori from Wallace & Hinkle (1996) compared with synthetic spectra generated by MOOG, using CNO abundances from Lambert et al. (1984), model atmosphere from Plez (1992), and stellar parameters listed in Table 1. The error bars come from the difference of observations taken in two epochs. We overplot a synthetic spectrum (*thick line*) derived using the Fe abundances listed in Table 5 and synthetic spectra (*thin lines*) computed with Fe abundances different by ±0.20 dex , which corresponds to the typical uncertainty in [Fe/H] for a solar neighborhood cool, luminous star. Fe lines and their wavelengths in Å are marked (*bold vertical lines*) at the top of each panel. CN, Sc, and unidentified lines (*question marks*) are also marked (*vertical lines*). Tick marks along the *x*-axis are 1 Å apart. The [Fe/H] value from Table 5 for each line is given in each panel.

from the literature. Some effective temperatures come from spectroscopic measurements (Luck 1982a, 1982b; Luck & Bond 1989; Carr et al. 2000). Other effective temperatures come from the calibration of $V-K$ colors versus $T_{\rm eff}$, where $T_{\rm eff}$ comes from angular diameters measured by infrared interferometry (Smith & Lambert 1985, 1986). α Ori has a $T_{\rm eff}$ determination from its angular diameter measured by infrared interferometry ($T_{\rm eff} = 3605 \pm 43$ K; Dyck, van Belle, & Thompson 1998), which is very good agreement with the spectroscopic value obtained by Carr et al. (2000) ($T_{\rm eff} = 3540 \pm 260$; see Table 1).

For IRS 7, the brightest infrared source in the GC, Carr et al. (2000) determined $T_{\rm eff}$ spectroscopically by requiring the carbon abundance derived from CO lines to be independent of the lower excitation potential. We adopt the stellar parameters for IRS 7 from Carr et al. (2000), which were derived using the standard Plez grid of model atmospheres. Their $T_{\rm eff}$ analysis relied largely on the second-overtone CO lines present in the H band (1.5–1.8 μm), because most of the first-overtone CO lines present in the K band are saturated.

For the remaining nine stars in the GC, the H-band spectra are too faint to be observed with CSHELL at the IRTF because of high extinction. Therefore CO cannot be used to compute the effective temperature. For those nine GC stars, broad molecular bands present in H- and K-band low-resolution spectra ($\lambda/\Delta\lambda \sim 500$) are used to estimate $T_{\rm eff}$ (S. V. Ramírez, R. D. Blum, & K. Sellgren 2000, in preparation). These features are CO (2.3 μm) and H_2O (1.9 μm). The CO strength increases with decreasing $T_{\rm eff}$ and decreasing surface gravity (log g). The H_2O strength also increases with decreasing $T_{\rm eff}$ but increases with increasing log g. These two features together, therefore, provide two-dimensional spectral classification (Baldwin, Frogel, & Persson 1973; Kleinmann & Hall 1986; Blum, Sellgren & DePoy 1996b). The low-resolution spectra of GC stars were taken with the IRS at CTIO, used in cross-dispersed mode to acquire the H and K bands simultaneously (S. V. Ramírez, R. D. Blum, & K. Sellgren 2000, in preparation). Nearby late-type stars with $T_{\rm eff}$ determinations based directly or indirectly on the infrared interferometry technique (Smith & Lambert 1985, 1986, 1990; Fernández-Villacañas, Rego, & Cornide 1990; McWilliam 1990; Dyck et al. 1998; Richichi et al. 1998) were observed to calibrate our $T_{\rm eff}$ determination. The low-resolution spectra of cool, luminous stars with known $T_{\rm eff}$ were taken with the IRS at CTIO and with TIFKAM at MDM Observatory (S. V. Ramírez, R. D. Blum, & K. Sellgren 2000, in preparation). The distinction between giants and supergiants is determined by the presence or weakness of H_2O, respectively. The CO index is computed in the same way as in Blum et al. (1996b). Once the distinction between giants and supergiants is established, $T_{\rm eff}$ is determined from the relations shown in Figure 2, which are the best unweighted linear fit to the data. VR 5-7, IRS 19, IRS 22, BSD 72, BSD 124, and BSD 129 were classified as supergiant stars, and IRS 11, BSD 114, and BSD 140 were classified as giant stars. The luminosity class for GC stars is also listed in Table 3. Our values for $T_{\rm eff}$ for GC stars agree with the results from Blum et al. (1996b), for the stars that are common to both samples. Our value for $T_{\rm eff}$ from the CO index of IRS 7, 3400 ± 300 K, is also in good agreement with the spectroscopic value of $T_{\rm eff}$ from Carr et al. (2000), 3470 ± 250 K. IRS 7 has a low carbon abundance (Carr et al. 2000, [C/H] $= -0.8$). The good agreement between the $T_{\rm eff}$ from CO

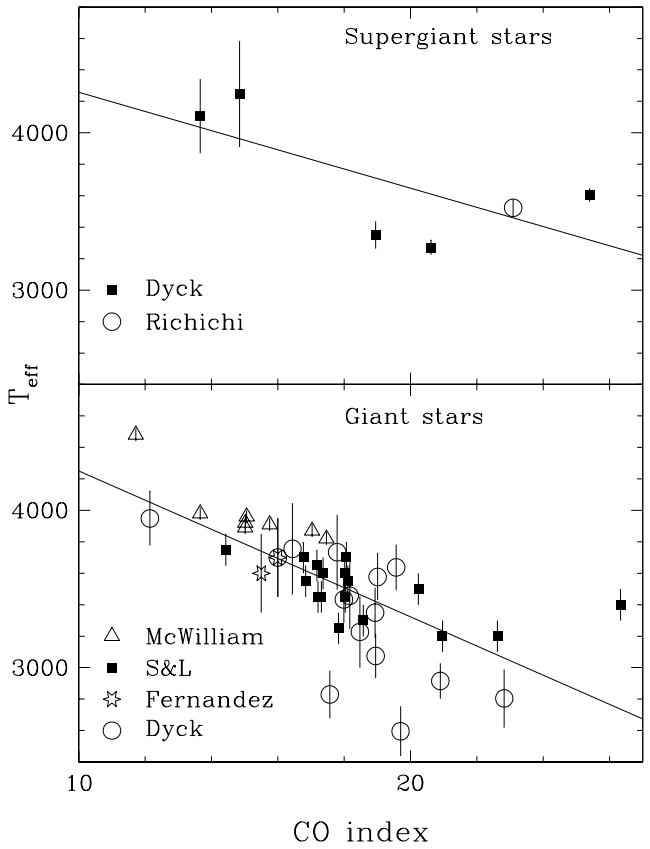

FIG. 2.—CO index vs. effective temperature, $T_{\rm eff}$, for supergiant and giant stars. *Upper panel*: The calibration for supergiant stars, with $T_{\rm eff}$ from Dyck et al. (1998) (*filled squares*) and Richichi et al. (1998) (*open circles*), both measured from infrared interferometry. *Lower panel*: The calibration for giant stars. Values of $T_{\rm eff}$ from McWilliam (1990) (*open triangles*), Smith & Lambert (1985, 1986, 1990) (*filled circles*), and Fernández-Villacañas et al. (1990) (*open stars*) are derived from a relationship between $V-K$ and $T_{\rm eff}$ measured by infrared interferometry. $T_{\rm eff}$ from Dyck et al. (1998) (*open circles*) are derived from infrared interferometry measurements. In both panels the uncertainties come from the literature. The best unweighted linear fit to the data (*solid lines*) is used to compute the $T_{\rm eff}$ of the Galactic center stars.

index and the spectroscopic $T_{\rm eff}$ suggests that our derived values of $T_{\rm eff}$ are not strongly affected by moderate variations in the abundance of carbon. The typical uncertainty in $T_{\rm eff}$ computed from the CO index is 300 K for supergiants and 280 K for giants. The $T_{\rm eff}$ for cool, luminous stars in the solar neighborhood is listed in Table 1 and for GC stars is listed in Table 3.

3.2.2. *Surface Gravity*

For the cool, luminous stars in the solar neighborhood, the surface gravity, g, from the literature was used (Luck 1982a, 1982b; Smith & Lambert 1985, 1986; Luck & Bond 1989; Carr et al. 2000). For the GC stars, the surface gravity is determined from the relation

$$\log g = \log (M/M_\odot) + 4 \log (T_{\rm eff}/T_{\rm eff\odot}) - \log (L/L_\odot) - \log g_\odot \, . \quad (1)$$

$T_{\rm eff}$ has been already determined. The luminosity, L, is computed from $M_{\rm bol}$, which is determined from K, A_K, the GC distance, and the bolometric correction, BC. A GC distance of 8 kpc is assumed (Reid 1993), K and A_K are from Blum et al. (1996a), and the BC is taken from Elias, Frogel, & Humphreys (1985). The final $M_{\rm bol}$ for the GC stars is listed

in Table 3. The uncertainty in M_{bol} from the GC stars comes mainly from uncertainties in the extinction curve, $E(H-K)/A_K$, and it is estimated to be ± 0.4 (Carr et al. 2000). Once M_{bol} and T_{eff} are determined, the stars are placed in the H-R diagram, and masses, M, are obtained by overplotting evolutionary tracks of varying initial masses. Solar metallicity evolutionary tracks (Schaller et al. 1992) are used to determine masses for supergiant stars. For the coolest stars, that fall outside the T_{eff} range of Schaller et al. (1992) evolutionary tracks, asymptotic giant branch (AGB) tracks from Marigo, Bressan, & Chiosi (1996) were used to estimate their masses. Note that the stellar evolution models assume mass loss for the more massive stars, and the current mass of the star at its present age is assumed. Twice solar metallicity evolutionary tracks (Schaerer et al. 1993) gave the same result for the derived masses. The value of log g for GC stars is listed in Table 3. The uncertainty is estimated considering the uncertainties in mass, effective temperature, and luminosity. Figure 3 shows the H-R diagram of GC stars and also the cool, luminous stars in the solar neighborhood. It is seen that the GC stars and the cool, luminous stars in the solar neighborhood occupy the same place in the H-R diagram and hence are very similar types of stars.

3.2.3. *Microturbulent Velocity*

The values for the microturbulent velocity (ξ) for the cool, luminous stars found in the literature show considerable

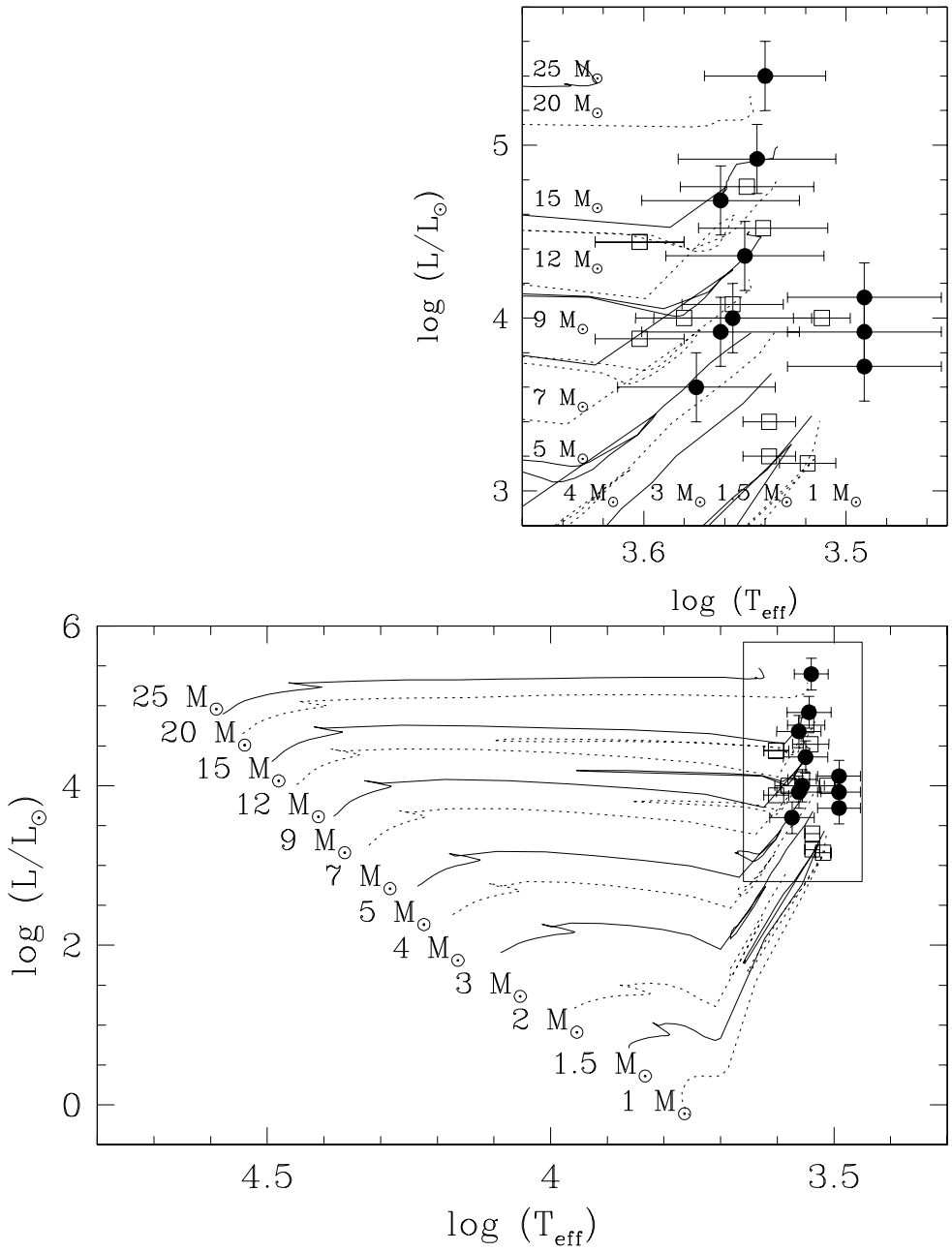

FIG. 3.—H-R diagram of Galactic center (GC) stars (*filled circles*) and cool, luminous stars in the solar neighborhood (*open squares*). Stellar parameters and their uncertainties are given in Tables 1 and 3. Solar metallicity evolutionary tracks (Schaller et al. 1992) are overplotted to determine masses for GC stars. The GC stars and the cool, luminous stars in the solar neighborhood occupy the same place in the H-R diagram and hence are very similar types of stars.

variation among authors. Carr et al. (2000) found for VV Cep (HR 8383) a much lower value ($\xi = 3.7 \pm 0.2$ km s^{-1}) than the one from Luck (1982b), $\xi = 5.0 \pm 0.5$ km s^{-1}. Carr et al. (2000) used CO lines of the same excitation potential, for which the carbon abundance should be independent of the equivalent widths of the lines when ξ is correct. Luck (1982b) used the same principle but used Fe I lines instead of CO lines.

Seven of our Fe I lines have similar excitation potential, and those lines were used to derive the microturbulence for the cool, luminous stars in the solar neighborhood. This was done in an iterative way. An Fe abundance was derived from the synthetic model of cool, luminous stars in the solar neighborhood, which included lines of Fe, CN, and other lines. Using the derived Fe abundance, a synthetic model was computed containing only Fe lines, and an equivalent width was measured for the Fe lines. This way the equivalent width is free from contributions from CN or other species. Then, the derived Fe abundances from the synthesis were plotted versus the Fe equivalent widths. This process was repeated with different microturbulent velocities until the Fe abundance was independent of the Fe equivalent width. The final equivalent widths of the Fe lines used in this process are listed in Table 4. The obtained value of ξ for cool, luminous stars in the solar neighborhood is listed in Table 1. The uncertainty in the obtained microturbulent velocity comes from the uncertainty in the slope in the graph of Fe abundance versus equivalent width, based on the scatter of the data points. Our value of ξ for α Ori ($\xi = 2.8 \pm 0.2$) is slightly different from the value of ξ from Carr et al. (2000) ($\xi = 3.23 \pm 0.15$). There is good agreement between our values of ξ and the ones given by Smith & Lambert (1985, 1986), where the mean difference is 0.15 km s^{-1}. Our values of ξ are systematically lower than the values given by Luck (1982b) and Luck & Bond (1989) (HR 8383, HD 202380, HD 163428, BD +59°594, HD 232766), where the mean difference is 2.4 km s^{-1}. Our value of ξ for HR 8726 is in good agreement with the value given by Luck (1982a).

We do not have sufficient S/N for the GC stars to apply this technique for finding ξ. Instead, to get the microturbulent velocity for the GC stars, a relation between log g and ξ is used. McWilliam (1990) showed that log g and ξ are related in G and K giants. The values of ξ and log g for cool, luminous stars in the solar neighborhood, including the values from Carr et al. (2000) and Smith & Lambert (1985, 1986, and 1990), are plotted to get a relation to apply to the GC stars. Figure 4 shows this relation for stars with $T_{\rm eff}$ and log g similar to those of the GC stars. An unweighted linear fit to the data gives

$$\xi = (2.78 - 0.82 \times \log g) \text{ km s}^{-1} . \quad (2)$$

The uncertainty in the microturbulent velocity is estimated from the uncertainty of the fit (± 0.4 km s^{-1}) and the uncertainty from the surface gravity. The value of ξ for IRS 7 obtained by this fit, $\xi = 3.3 \pm 0.4$ km s^{-1}, is in good agreement with the value of ξ from Carr et al. (2000), $\xi = 3.30 \pm 0.34$ km s^{-1}, obtained using CO lines.

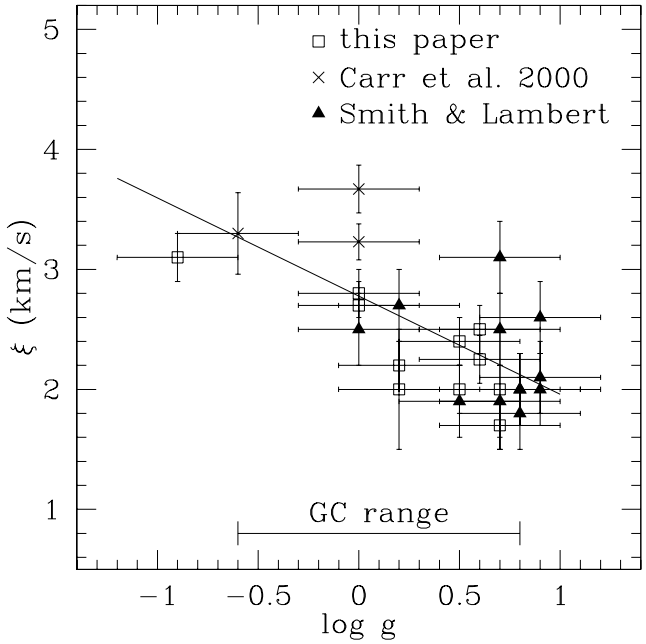

FIG. 4.—Relation between microturbulent velocity (ξ) and surface gravity (log g). Values of ξ and log g are from Table 1 of this paper (*open squares*), Carr et al. (2000) (*crosses*), and Smith & Lambert (1985, 1986, 1990) (*filled triangles*). The best unweighted linear fit to the data (*solid line*) is used to compute ξ for the GC stars.

3.2.4. *Macroturbulent Velocity*

The synthetic spectra have to be convolved with a macroturbulent broadening function (Gray 1992, p. 405), and with instrumental broadening, to match the line widths of the

TABLE 4

Fe II EQUIVALENT WIDTHS FOR NEARBY LATE-TYPE STARS[a]

STAR	WAVELENGTH OF Fe I LINES (Å)						
	22381.3	22386.9	22391.2	22399.0	22818.8	22838.6	22852.2
HR 6146	90±6	355±8	162±7	210±7	130±6	277±7	211±7
HR 6702	67±5	332±9	136±7	189±7	119±6	234±7	220±7
HR 7442	60±5	339±9	143±8	174±8	141±8	294±8	246±8
HR 8062	65±5	351±9	149±7	199±6	110±6	208±7	...
α Ori.....	101±8	520±10	218±10	319±10	178±10	339±10	271±10
HD 202380.....	102±8	476±11	180±9	311±9	137±8	299±9	...
HR 8383	86±7	466±10	183±9	285±9	112±8	261±9	233±9
HD 163428.....	87±7	430±9	172±9	241±9	113±8	263±8	...
BD +59°594.....	107±9	522±11	171±12	329±12	96±9	289±13	226±12
HD 232766.....	66±6	410±8	159±9	228±9	97±8	216±9	173±9
HR 8726	71±6	397±8	158±8	234±8	115±8	239±8	186±8

[a] Equivalent widths of each Fe I line (mÅ).

observed spectrum. The instrumental broadening is a Gaussian of full width half-maximum given by the spectral resolution of the instrument (7 km s^{-1}). CN lines in two bands (21798–21804 Å; 22403–22409 Å) were used to determine the macroturbulent velocity (ζ) for the cool, luminous stars in the solar neighborhood. Several synthetic spectra were generated by MOOG using different values of ζ and N abundances. Then, χ^2 was computed for each synthetic spectrum, and the best set of N abundance and ζ was chosen for the minimum χ^2. Note that this procedure is not measuring ζ but rather is determining the best line broadening that fits the data. Also, the N abundance obtained by this technique is not real because the C and O abundances have not been measured independently. Figure 5 shows the χ^2 contour maps, one for each band, for HR 8726. Figure 5 also shows the observed spectrum of HR 8726 and the synthetic spectrum for the values of ζ and N abundance that give a minimum χ^2 for both bands. The macroturbulent velocity for the cool, luminous stars in the solar neighborhood is given in Table 1. The uncertainty in ζ is given by the standard deviation of the values of ζ derived for each band. This uncertainty is more conservative than the uncertainty derived from χ^2 statistics.

For the GC stars, the same method was used for IRS 7, VR 5-7, IRS 19, IRS 22, and IRS 11. For the remaining stars, BSD 72, BSD 114, BSD 124, BSD 129, and BSD 140, only one band with CN lines was observed, and the band did not have enough S/N to carry out this method. The values of ζ in Table 1 were used to derive a relationship between log g and ζ for supergiant stars. Gray & Martin (1979) established a relationship between ξ and ζ for giant stars. McWilliam (1990) shows that ξ depends on log g, so by combining these two dependences we derive a relation between ζ and log g. The values of ζ for supergiant stars measured by the broadening of the CN lines are plotted versus log g to get a relation to apply to the fainter GC supergiant stars. Figure 6 shows this relation. An unweighted linear fit to the data gives

$$\zeta = (14.5 - 4.40 \times \log g) \text{ km s}^{-1} . \quad (3)$$

The uncertainty in the microturbulent velocity is estimated from the uncertainty of the fit (± 2.4 km s^{-1}) and the uncer-

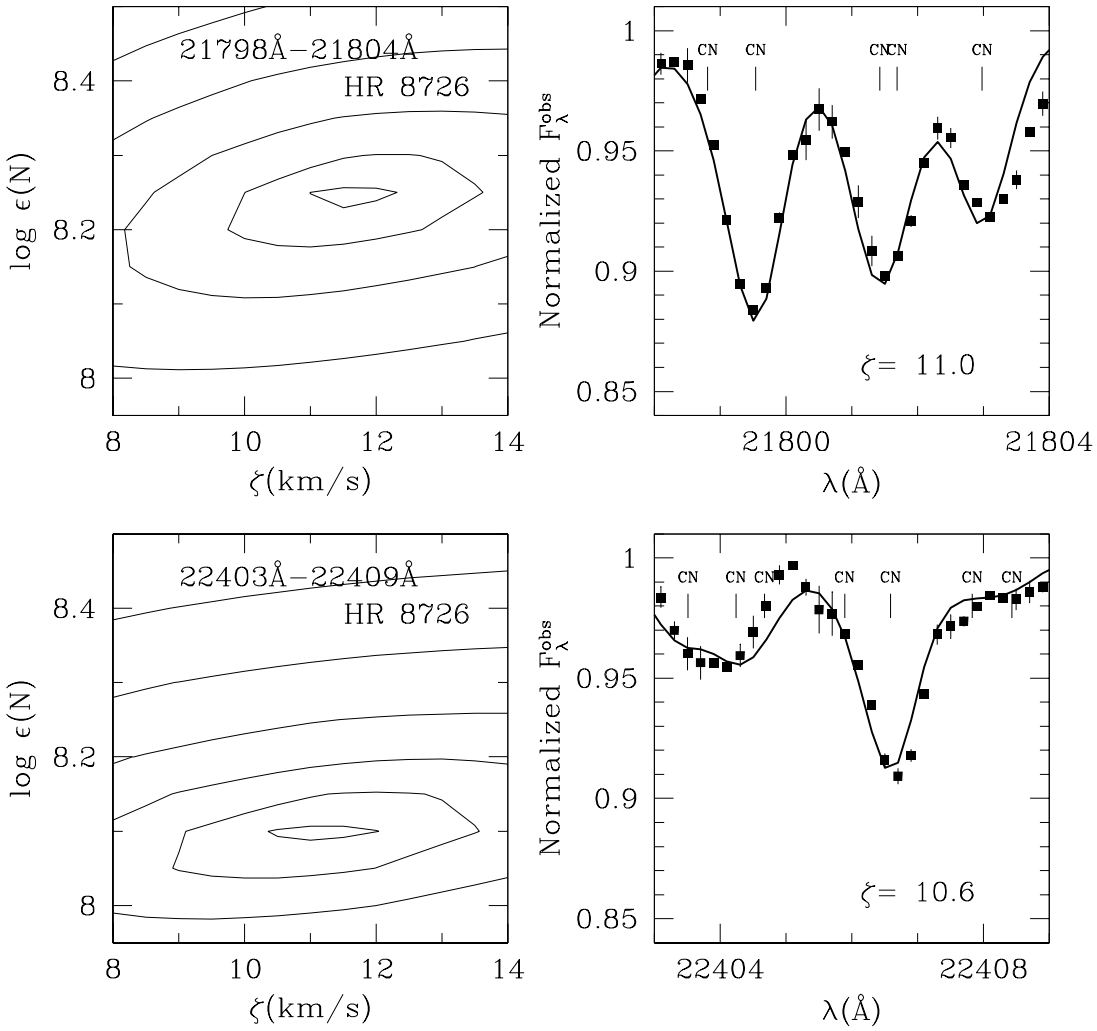

FIG. 5.—*Left-hand panels*: χ^2 contour maps for determining the nitrogen abundance, log ϵ (N), and macroturbulent velocity (ζ) for HR 8726. The minimum χ^2 gives the best set of log ϵ (N) and ζ for each set of CN lines (21798–21804 Å at the top, and 22403–22409 Å at the bottom). *Right-hand panels*: Observed spectrum of HR 8726 (*filled squares*) with error bars from the difference of observations taken at two positions along the slit and the synthetic spectrum of HR 8726 (*solid line*) using the derived log ϵ (N) and ζ for each CN band (21798–21804 Å at the top, and 22403–22409 Å at the bottom). The synthetic spectrum is calculated by MOOG, using stellar parameters in Table 1 and a model atmosphere from Plez (1992). The value of log ϵ (N) derived by this technique is not a true nitrogen abundance, because a combination of C and N abundances are needed to derive a true value of log ϵ (N) from CN lines.

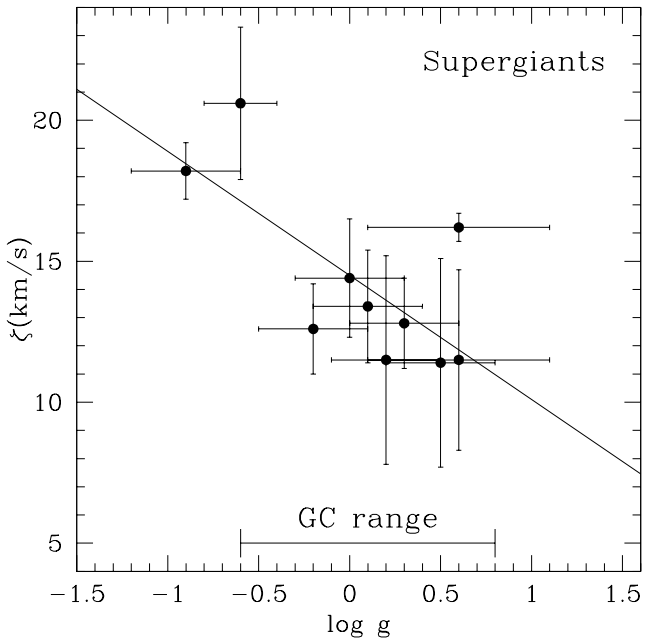

FIG. 6.—Relation between macroturbulent velocity (ζ) and surface gravity (log g) for supergiant stars (*filled circles*). All supergiant stars from Table 1 and IRS 7, VR 5-7, IRS 19, and IRS 22 from Table 3 are plotted. The best unweighted linear fit to the data (*solid line*) is used to compute ζ for the GC supergiant stars BSD 72, BSD 124, and BSD 129.

tainty in the surface gravity. Equation (3) was applied to BSD 72, BSD 124, and BSD 129.

For giant stars, the range in log g is too narrow to derive a relationship. A mean value of $\zeta = 9.0 \pm 3.0$ km s^{-1} is used for the GC giant stars. This mean value is derived from values of ζ for solar neighborhood giant stars and IRS 11 measured by the broadening of the CN lines, as given in Tables 1 and 3. This mean value was adopted for BSD 114 and BSD 140.

3.3. *Uncertainties*

Our basic observable parameters, $T_{\rm eff}$ and $M_{\rm bol}$, have uncertainties that come from the technique used to compute them (§§ 3.2.1 and 3.2.2). The surface gravity uncertainty includes both the uncertainty in $T_{\rm eff}$ and the uncertainty in $M_{\rm bol}$ (§ 3.2.2). The microturbulent velocity uncertainty includes both the uncertainties in log g and the uncertainty of the fit used to calculate it (§ 3.2.3). The same is true for the macroturbulent velocity (§ 3.2.4).

It is important to know what are the effects of each of these uncertainties in the abundance determination. The uncertainty in [Fe/H] for each stellar parameter has been estimated by varying one of the stellar parameters and computing the difference in iron abundance. A typical uncertainty in $T_{\rm eff}$ of ± 300 K results in an uncertainty of ∓ 0.08 dex in [Fe/H]. A typical uncertainty of ± 0.35 in log g implies an uncertainty of ± 0.12 dex in [Fe/H]. A typical uncertainty of ± 0.4 km s^{-1} in ξ causes an uncertainty of ∓ 0.09 dex in [Fe/H]. A typical uncertainty of ± 1.8 km s^{-1} in ζ translates to an uncertainty of ± 0.13 dex in [Fe/H]. The iron abundance is not very sensitive to uncertainties in $T_{\rm eff}$ and ξ, but it is more sensitive to uncertainties in log g and ζ. In addition to the uncertainty from the stellar parameters, the standard error must also be considered for each star. The standard error comes from the scatter in [Fe/H] as derived from individual Fe I lines. All the uncertainties from stellar parameters and the standard error for each star are listed in Tables 7 and 8. The total uncertainty is the quadratic addition of the uncertainties derived from the stellar parameters and the standard error in the value of [Fe/H] from individual Fe I lines. For the solar neighborhood stars and IRS 7, the quadratic addition of the uncertainties is a good estimation of the total uncertainty, because all the uncertainties come from independent measurements. In the cases in which ξ and ζ are computed through their relationships with log g, the uncertainties are not independent, and the quadratic addition can be an overestimation of the total uncertainty. We estimate that the total uncertainty will decrease by no more than 0.05 dex, if we consider the correlation of the uncertainties in log g, ξ, and ζ.

Systematic errors may be present as well. They may come from unidentified lines, which could make a contribution that is not included in our synthetic spectrum because of the lack of atomic and molecular parameters. They may also come from errors in the determination of *gf*-values or from failure of the model atmospheres to model the stars we observe correctly, because model atmospheres use solar abundance ratios, or NLTE effects.

3.4. *NLTE Effects*

The iron abundance could be affected by departures from LTE. The main NLTE effect in late-type stars is caused by overionization of electron donor metals by ultraviolet radiation (Auman & Woodrow 1975). Using the Saha equation, we found that in our typical star 93% of iron is neutral. Thus overionization should be smaller in our stars than in warmer giants, where only a few percent of iron is neutral.

It is known from empirical studies that abundances derived from low-excitation lines give systematically lower abundances (~ 0.3 dex) than the ones derived from high-excitation and ionized lines in late-type stars; high-excitation and ionized lines give very similar abundance results (Ruland et al. 1980; Steenbock 1985; Takeda 1991; Tomkin & Lambert 1983). Recently, Thévenin & Idiart (1999) studied NLTE effects in Fe abundances in metal-poor late-type stars. They found that ionized lines are not significantly affected by NLTE and that NLTE corrections become less important as [Fe/H] increases, being minimal for solar abundance stars. Mostly high-excitation lines are used in our analysis, so the NLTE effects that might be present should be minimal.

Tomkin & Lambert (1983) found that NLTE effects cancel out when a differential analysis is carried out relative to a very similar star in terms of effective temperature and luminosity. Nearby stars of similar effective temperature and luminosity as the GC stars (see Fig. 2) have been analyzed similarly in this paper, providing a differential abundance comparison that should remove any NLTE effects that might be present.

4. RESULTS

Each iron abundance value for a particular Fe I line and star was derived from a comparison between the synthetic spectrum generated by MOOG and the observed spectrum. The [Fe/H] results for each line for cool, luminous stars in the solar neighborhood and GC stars are listed in Table 5 and 6, respectively. The uncertainties per line are estimated from the ability to distinguish models with different [Fe/H]

TABLE 5

[Fe/H] FOR NEARBY LATE-TYPE STARS[a]

STAR	WAVELENGTH OF Fe I LINES (Å)							
	21781.8	22381.3	22386.9	22391.2	22399.0	22818.8	22838.6	22852.2
HR 6146	−0.05	+0.05	−0.20	0.00	−0.30	+0.15	+0.25	+0.10
HR 6702	−0.05	−0.05	−0.25	−0.05	−0.30	+0.20	+0.10	+0.30
HR 7442	+0.10	+0.10	−0.25	+0.10	−0.60	+0.20	+0.20	+0.20
HR 8062	+0.10	−0.10	−0.05	+0.05	−0.20	+0.10	−0.05	...
α Ori	+0.15	0.00	+0.05	+0.05	−0.10	+0.20	+0.10	0.00
HD 202380.....	+0.10	+0.10	+0.10	0.00	+0.10	+0.10	+0.10	...
HR 8383	−0.05	−0.10	−0.10	−0.10	−0.20	−0.15	−0.25	−0.10
HD 163428.....	+0.07	0.00	0.00	−0.02	−0.25	−0.05	−0.05	...
BD +59°594.....	−0.10	0.00	−0.25	−0.25	−0.25	−0.30	−0.35	−0.35
HD 232766.....	−0.10	−0.20	−0.15	−0.15	−0.40	−0.20	−0.40	−0.40
HR 8726	+0.15	−0.10	0.00	−0.05	−0.20	0.00	−0.10	−0.20

[a] Error in [Fe/H] for each line is ±0.05 dex; [Fe/H] determined from each Fe I line.

considering the S/N of the observed spectrum. For cool, luminous stars in the solar neighborhood, the uncertainty per line is estimated to be ±0.05 dex, since the S/N is very homogeneous among all lines and stars. For GC stars, the uncertainty is listed individually for each line in Table 6. Figures 1, 7, and 8 show the synthetic and observed spectra for each line for α Ori, cool, luminous stars in the solar neighborhood, and GC stars, respectively.

The final [Fe/H] results for each star are listed in Table 9. These values are the mean [Fe/H] weighted by the individual uncertainties in [Fe/H] for each Fe I line, as listed in Tables 5 and 6. The final uncertainty in Table 9 is the total uncertainty from Table 7 and 8.

The analyses of our paper and Carr et al. (2000) have five stars in common: IRS 7, α Ori, HR 6146 (30 Her), HR 6702, and HR 8383 (VV Cep). There is agreement in the Fe abundances within 0.1 dex for four stars (IRS 7, α Ori, HR 6146, and HR 8383). Our Fe abundance for HR 6702 is 0.18 dex lower than that of Carr et al. (2000). The abundance technique used in both studies is very similar, but Carr et al. (2000) included a different set of Fe I lines and slightly different stellar parameters.

IRS 7 is known to be a variable supergiant (Blum et al. 1996a). There is one Fe line common to the analysis of Carr et al. (2000) and of this paper, which was observed at different epochs by Carr et al. (2000) and by us. For this line, our result is consistent within the uncertainties with the results of Carr et al. (2000). Another spectrum of IRS 7, taken with NIRSPEC at the Keck Telescope 1 year after our observations, was kindly made available to us (D. F. Figer, private communication). We have one Fe line in common with the NIRSPEC spectrum, and again the iron abundance results from both data sets are also consistent within the uncertainties. We conclude that the effect of variability on our IRS 7 results are negligible considering our uncertainties.

TABLE 6

[Fe/H] FOR GALACTIC CENTER STARS[a]

STAR	WAVELENGTH OF Fe I LINES (Å)							
	21781.8	22381.3	22386.9	22391.2	22399.0	22818.8	22838.6	22852.2
IRS 7	+0.35	+0.22	−0.15	−0.10	—	+0.38	−0.30	...
	±0.05	±0.07	±0.10	±0.05		±0.05	±0.05	
VR 5-7.....	+0.12	+0.20	−0.30	+0.15	−0.40	+0.10	+0.15	...
	±0.03	±0.07	±0.10	±0.05	±0.10	±0.05	±0.07	
IRS 19	+0.30	+0.40	−0.30	+0.40	−0.05	+0.45	−0.05	...
	±0.05	±0.05	±0.10	±0.07	±0.10	±0.05	±0.10	
IRS 22	+0.30	−0.05	−0.40	+0.15	−0.40	+0.20	+0.35	+0.30
	±0.05	±0.05	±0.10	±0.10	±0.10	±0.10	±0.10	±0.10
BSD 124.....	...	+0.22	+0.20	+0.20	−0.10	+0.20	+0.20	...
		±0.07	±0.10	±0.20	±0.10	±0.05	±0.10	
BSD 129.....	...	+0.50	+0.50	+0.70	+0.20	+0.60	+0.60	...
		±0.20	±0.10	±0.20	±0.10	±0.10	±0.10	
BSD 72	...	+0.10	+0.40	+0.35	+0.05	+0.35	−0.20	...
		±0.10	±0.10	±0.10	±0.10	±0.10	±0.10	
BSD 114.....	...	−0.20	−0.85	−0.10	−0.70	0.00	−0.30	...
		±0.10	±0.20	±0.10	±0.10	±0.10	±0.10	
IRS 11	−0.15	+0.25	−0.80	−0.20	−0.80	−0.15	−0.50	...
	±0.05	±0.05	±0.10	±0.10	±0.10	±0.10	±0.10	
BSD 140.....	...	0.00	−0.40	+0.10	−0.40	0.00	0.00	...
		±0.20	±0.20	±0.20	±0.20	±0.10	±0.10	

[a] [Fe/H] determined from each Fe I line.

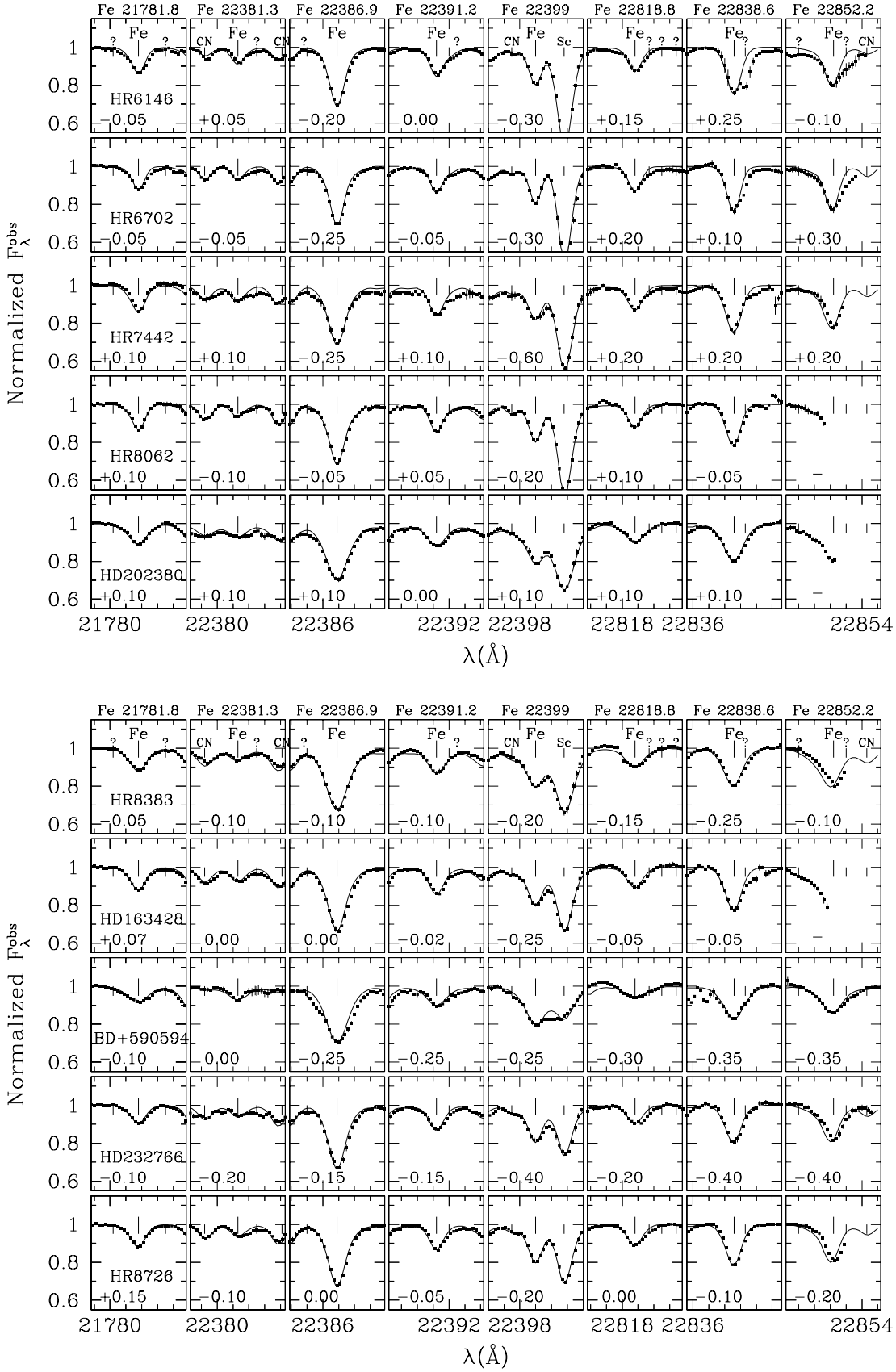

FIG. 7.—Observed (*filled squares*) and synthetic spectra (*solid line*) for cool, luminous stars in the solar neighborhood. The synthetic spectrum is computed by MOOG, using the stellar parameters listed in Table 1 and model atmospheres from Plez (1992). The error bars come from the difference of observations taken at two positions along the slit. Fe lines and their wavelengths in Å are marked (*bold vertical lines*) at the top panels. CN, Sc, and unidentified lines (*question marks*) are also marked (*vertical lines*). Tick marks along the *x*-axis are 1 Å apart. The [Fe/H] value from Table 5 for each line is given in each panel.

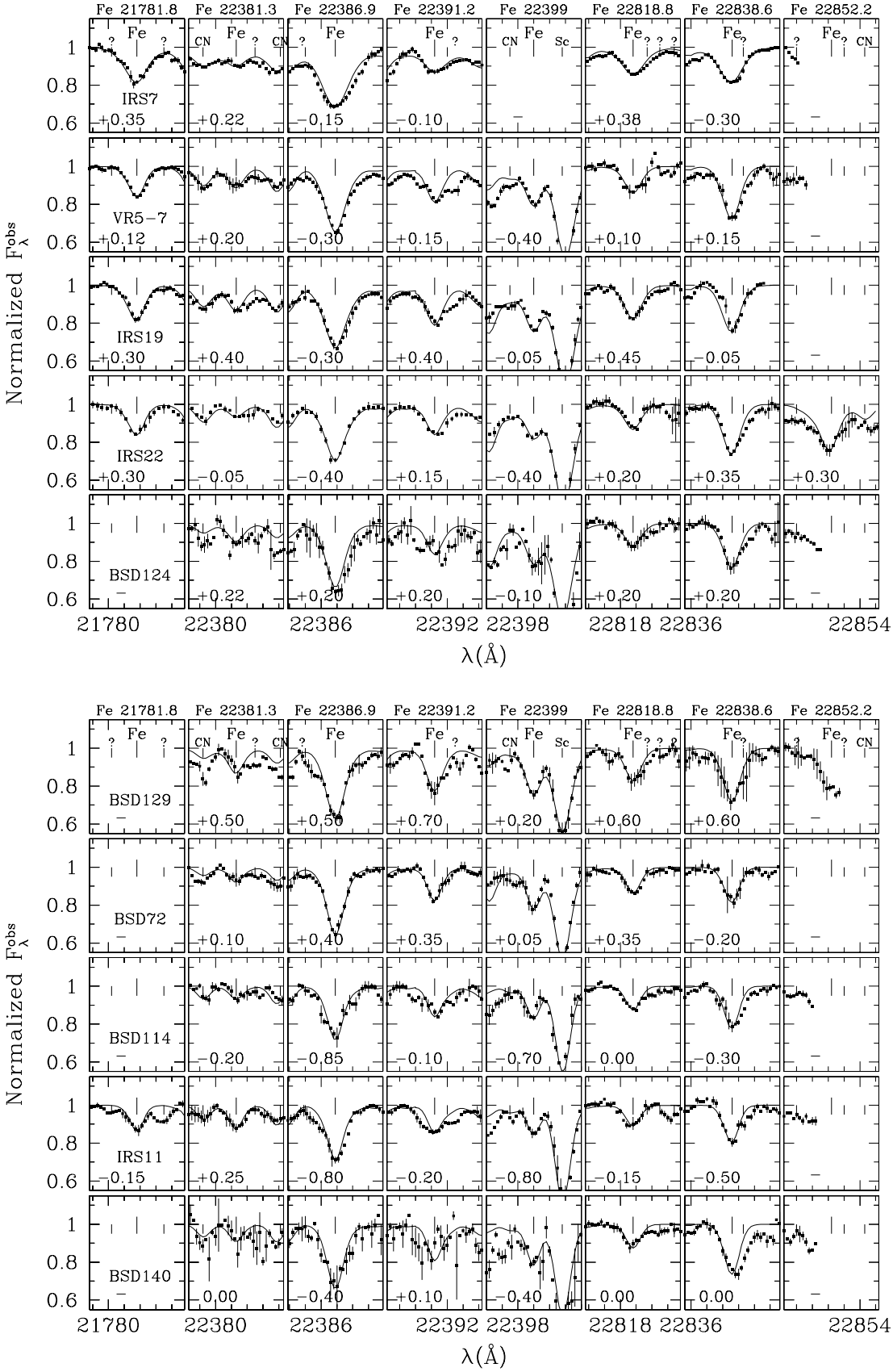

FIG. 8.—Similar to Fig. 7, except these are observed and synthetic spectra for Galactic center stars, using stellar parameters given in Table 3. Symbols are the same as Fig. 7. The [Fe/H] value from Table 6 for each line is given in each panel.

TABLE 7

UNCERTAINTIES IN [Fe/H] FOR SOLAR NEIGHBORHOOD STARS

Star	$\pm T_{\rm eff}$[a]	$\pm\log g$[a]	$\pm\xi$[a]	$\pm\zeta$[a]	Std.[b]	Total[c]
HR 6146	$\mp$0.03	$\pm$0.10	$\mp$0.11	$\pm$0.08	$\pm$0.07	$\pm$0.19
HR 6702	$\mp$0.03	$\pm$0.10	$\mp$0.11	$\pm$0.13	$\pm$0.08	$\pm$0.22
HR 7442	$\mp$0.03	$\pm$0.10	$\mp$0.04	$\pm$0.19	$\pm$0.11	$\pm$0.25
HR 8062	$\mp$0.03	$\pm$0.10	$\mp$0.04	$\pm$0.04	$\pm$0.04	$\pm$0.13
α Ori	$\mp$0.07	$\pm$0.10	$\mp$0.04	$\pm$0.04	$\pm$0.03	$\pm$0.14
HD 202380.....	$\mp$0.05	$\pm$0.17	$\mp$0.04	$\pm$0.04	$\pm$0.02	$\pm$0.19
HR 8383	$\mp$0.07	$\pm$0.10	$\mp$0.04	$\pm$0.15	$\pm$0.03	$\pm$0.20
HD 163428.....	$\mp$0.05	$\pm$0.17	$\mp$0.04	$\pm$0.22	$\pm$0.04	$\pm$0.29
BD +59°594.....	$\mp$0.05	$\pm$0.10	$\mp$0.04	$\pm$0.07	$\pm$0.05	$\pm$0.15
HD 232766.....	$\mp$0.05	$\pm$0.10	$\mp$0.04	$\pm$0.26	$\pm$0.05	$\pm$0.29
HR 8726	$\mp$0.05	$\pm$0.10	$\mp$0.04	$\pm$0.04	$\pm$0.04	$\pm$0.13

[a] $T_{\rm eff}$ = effective temperature; g = surface gravity; ξ = microturbulent velocity; ζ = macroturbulent velocity.

[b] Standard error, determined from scatter among [Fe/H] values measured for different Fe I lines.

[c] Total uncertainty, derived from quadratic sum of uncertainties due to the standard error and the uncertainties from the stellar parameters ($T_{\rm eff}$, log g, ξ, ζ).

4.1. *Galactic Center Mean* [Fe/H]

An unweighted mean value of [Fe/H] = +0.09 is obtained for the GC stars. A mean weighted by the total uncertainties in [Fe/H] (Table 9) gives a value of [Fe/H] = +0.12 for the GC stars. The estimated dispersion or σ is 0.22 dex, which is not significantly different from the typical total uncertainty in [Fe/H] for each GC star of 0.28 dex. Even if the total uncertainties are overestimated by

TABLE 8

UNCERTAINTIES IN [Fe/H] FOR GALACTIC CENTER STARS

Star	$\pm T_{\rm eff}$[a]	$\pm\log g$[a]	$\pm\xi$[a]	$\pm\zeta$[a]	Std.[b]	Total[c]
IRS 7	$\mp$0.07	$\pm$0.07	$\mp$0.09	$\pm$0.19	$\pm$0.13	$\pm$0.27
VR 5-7.....	$\mp$0.08	$\pm$0.10	$\mp$0.11	$\pm$0.11	$\pm$0.11	$\pm$0.23
IRS 19	$\mp$0.08	$\pm$0.10	$\mp$0.11	$\pm$0.14	$\pm$0.13	$\pm$0.26
IRS 22	$\mp$0.08	$\pm$0.10	$\mp$0.11	$\pm$0.11	$\pm$0.12	$\pm$0.24
BSD 124.....	$\mp$0.08	$\pm$0.10	$\mp$0.11	$\pm$0.19	$\pm$0.06	$\pm$0.26
BSD 129.....	$\mp$0.08	$\pm$0.10	$\mp$0.11	$\pm$0.19	$\pm$0.08	$\pm$0.27
BSD 72	$\mp$0.08	$\pm$0.10	$\mp$0.11	$\pm$0.19	$\pm$0.10	$\pm$0.27
BSD 114.....	$\mp$0.08	$\pm$0.17	$\mp$0.13	$\pm$0.21	$\pm$0.16	$\pm$0.35
IRS 11	$\mp$0.08	$\pm$0.17	$\mp$0.13	$\pm$0.15	$\pm$0.18	$\pm$0.33
BSD 140.....	$\mp$0.08	$\pm$0.17	$\mp$0.13	$\pm$0.21	$\pm$0.10	$\pm$0.32

[a] $T_{\rm eff}$ = effective temperature; g = surface gravity; ξ = microturbulent velocity; ζ = macroturbulent velocity.

[b] Standard error, determined from scatter among [Fe/H] values measured for different Fe I lines.

[c] Total uncertainty, derived from quadratic sum of uncertainties due to the standard error and the uncertainties from the stellar parameters ($T_{\rm eff}$, log g, ξ, ζ).

TABLE 9

MEAN [Fe/H] FOR EACH STAR

SOLAR NEIGHBORHOOD STARS			GALACTIC CENTER STARS		
Star	$N_{\rm lines}$	[Fe/H][a]	Star	$N_{\rm lines}$	[Fe/H][a]
HR 6146	8	-0.01 ± 0.19	IRS 7	6	$+0.09\pm0.27$
HR 6702	8	-0.02 ± 0.22	VR 5-7[b].....	7	$+0.09\pm0.23$
HR 7442	8	$+0.01\pm0.25$	IRS 19	7	$+0.29\pm0.26$
HR 8062	7	-0.03 ± 0.13	IRS 22	8	$+0.09\pm0.24$
α Ori	8	$+0.05\pm0.14$	BSD 124.....	6	$+0.17\pm0.26$
HD 202380.....	7	$+0.07\pm0.19$	BSD 129.....	6	$+0.49\pm0.27$
HR 8383	8	-0.14 ± 0.20	BSD 72	6	$+0.17\pm0.27$
HD 163428.....	7	-0.05 ± 0.29	BSD 114.....	6	-0.29 ± 0.35
BD +59°594.....	8	-0.24 ± 0.15	IRS 11	7	-0.16 ± 0.33
HD 232766.....	8	-0.26 ± 0.29	BSD 140.....	6	-0.06 ± 0.32
HR 8726	8	-0.07 ± 0.13			

[a] Error in [Fe/H] is the total uncertainty from Tables 7 and 8.

[b] M supergiant star in the Quintuplet cluster (R = 30 pc).

~ 0.05 dex by the quadratic addition of the individual uncertainties, the typical uncertainty per star does not get small enough to resolve the [Fe/H] distribution (see § 3.3). This means that the dispersion of the GC [Fe/H] distribution can be understood by the uncertainties present in the data.

Note that the supergiant VR 5-7, at $R = 30$ pc, has [Fe/H] $= +0.09 \pm 0.22$, which is similar to the supergiants at $R < 2.5$ pc, which have a mean [Fe/H] $= +0.21 \pm 0.15$.

An unweighted mean of [Fe/H] $= -0.05$ and a mean weighted by the total uncertainties of [Fe/H] $= +0.03$ was obtained for the 11 cool, luminous stars in the solar neighborhood. The estimated dispersion or σ is 0.16 dex, which again is not significantly different from the typical total uncertainty in [Fe/H] which is 0.20 dex for these stars.

The obtained mean [Fe/H] for the GC is close to solar and, furthermore, very similar to the cool, luminous stars in the solar neighborhood that were analyzed in the same way.

5. DISCUSSION

Our mean [Fe/H] for the GC stars, $+0.12 \pm 0.22$, is similar to that of supergiants in the Galactic disk. Figure 9*a* compares the GC [Fe/H] distribution with the [Fe/H] distribution of 40 F, G, K, and M supergiants within 2 kpc of the Sun (Luck & Bond 1989). The mean [Fe/H] of the solar neighborhood supergiant stars from (Luck & Bond 1989) is $+0.13$ with a dispersion of 0.20 dex. The width and mean of the two distributions agree closely. In Figure 9*b*, we compare the GC [Fe/H] distribution with that of the 11 cool supergiants and luminous giants we have analyzed in this paper. Again, the mean and width of the [Fe/H] distribution for the GC stars and solar neighborhood stars are consistent. Unlike the Luck & Bond (1989) sample of supergiants, our 11 nearby stars are restricted to the same range in stellar parameter space as the GC sample; in addition, we have used the same analysis method, Fe I lines, and stellar models for all the stars. It is important to emphasize that this differential analysis makes the abundance comparison between our samples of GC and nearby stars robust against possible systematic errors that might effect the absolute values of [Fe/H]. Hence, we can conclude that the Fe abundances for the sample of GC stars in this paper are nearly identical to those of similar $T_{\rm eff}$ and luminosity stars in the solar neighborhood, with no evidence for a supersolar metallicity.

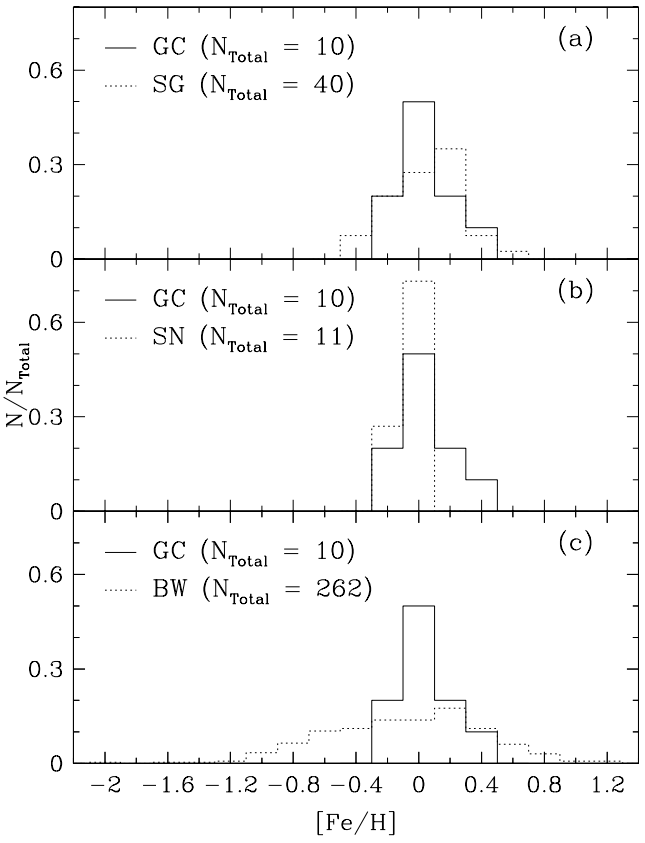

FIG. 9.—(*a*) Fractional distribution of [Fe/H] for 10 GC stars (*solid line*) compared to [Fe/H] for 40 solar neighborhood supergiant stars (*dashed line*) from Luck & Bond (1989). (*b*) Fractional distribution of [Fe/H] for 10 GC stars (*solid line*) compared to [Fe/H] for 11 solar neighborhood stars observed and analyzed in this paper (*dashed line*). (*c*) Fractional distribution of [Fe/H] for 10 GC stars (*solid line*) compared to [Fe/H] for 262 Baade's window stars (*dashed line*) from Sadler et al. (1996).

Our mean [Fe/H] for the GC stars of $+0.12 \pm 0.22$ appears to be in conflict with the iron abundance of the Pistol star, at $R = 30$ pc in the Quintuplet cluster. Najarro et al. (1999) derive [Fe/H] ~ 0.5 for the Pistol star. They qualify their result as preliminary, since details of the atmosphere modeling, such as the effects of charge exchange reactions, have to be studied and included in future work. The Pistol star abundance is derived from emission lines in the winds from this hot star, so the atmospheric modeling techniques are fundamentally different from those more established techniques we have used to study abundances from photospheric absorption lines in cool giant or supergiant stars.

Serabyn & Morris (1996) have proposed that the central cluster was built up by continuous, perhaps episodic, star formation over the lifetime of the Galaxy. In this case, the central 100 pc would form a stellar population distinct from the old population of the Bulge. In Figure 9*c*, the GC [Fe/H] distribution is compared with the [Fe/H] distribution for 262 stars in Baade's window (BW) in the bulge ($l, b = 1°, -4°$; Sadler, Rich, & Terndrup 1996). Sadler et al. (1996) have a typical uncertainty per star of ± 0.2 dex, so their finding that [Fe/H] ranges from -1.0 to $+0.5$ in BW shows the abundance spread of BW's distribution is well resolved by their technique. The distribution of [Fe/H] in the GC, however, has a similar width as the uncertainties in [Fe/H], 0.28 dex per star. Stars as metal-rich or as metal-poor as observed in the Bulge are not found in our sample of GC stars. However, our GC stars are restricted to a young to intermediate-age population, and hence an old stellar population, if it exists in the central 100 pc, is not sampled by the work of this paper. A larger abundance spread could be represented in such an older population, but a spectroscopic abundance analysis will require the sensitivity to reach K and M giants. A more complete comparison must also include measurements of the abundance patterns in the central regions relative to the Bulge. For example, the Bulge K giants analyzed by McWilliam & Rich (1994) show a distinct enhancement in the α elements, compared to Fe.

An IMF weighted toward more massive stars in the GC has been proposed by Morris & Serabyn (1996). Recently, Figer et al. (1999) have found an IMF slanted towards massive stars for the Arches and Quintuplet clusters, both

located within 30 pc of the GC. A history of chemical evolution dominated by massive stars is expected to result in enhancements of oxygen and α elements, such as Mg, Si, Ca, and Ti, relative to Fe (Wheeler, Sneden, & Truran 1989). The next step of our GC project is to measure abundances of α elements and study selective enrichment in the GC.

Chemical evolution models try to explain abundance patterns by considering the relative star formation rate, the gas infall and outflow rates, the star formation history, and the abundance of the gas compared to the stars (see Audouze & Tinsley 1976; Rana 1991). Most chemical evolution models that reproduce the radial gradients in galaxies are valid only for distances greater than 2 kpc from the Galactic center (Tinsley & Larson 1978; Samland, Hensler, & Theis 1997; Chiappini, Matteucci, & Padoan 2000; Portinari & Chiosi 1999). Now that the molecular gas in the GC (from which stars form) has been extensively studied (Stark et al. 1991; Blitz et al. 1993; Morris & Serabyn 1996) and that the abundances of stars in the GC has been obtained for the first time, we strongly urge theoreticians to put all these data together into a detailed chemical evolution model describing the central parsecs of our Galaxy.

6. CONCLUSIONS

We present the first measurement of stellar [Fe/H] for 10 stars in the Galactic center (GC), at distances from the GC of $R < 30$ pc. Nine GC stars are located in the central cluster ($R < 2.5$ pc), and one star is located in the Quintuplet cluster ($R = 30$ pc). The abundance analysis is based on high-resolution ($\lambda/\Delta\lambda = 40{,}000$) K-band spectra. The mean [Fe/H] of the GC is determined to be near solar, $[\mathrm{Fe/H}] = +0.12 \pm 0.22$, and also similar to the mean [Fe/H] for cool, luminous stars in the solar neighborhood, $[\mathrm{Fe/H}] = +0.03 \pm 0.16$, observed and analyzed in the same way. The width of the GC [Fe/H] distribution, which ranges from $[\mathrm{Fe/H}] = -0.3$ to $+0.5$, is found to be significantly narrower than the width of the [Fe/H] distribution of Baade's window, which ranges from $[\mathrm{Fe/H}] = -1.0$ to $+0.8$. The GC [Fe/H] distribution is consistent with the [Fe/H] distribution of supergiant stars in the solar neighborhood. This suggests that the most luminous stars in the GC are unlikely to be dominated by bulgelike stars and that the evolutionary path of the GC, while unique, is closer to the disk's than to the bulge's. The Quintuplet star at $R = 30$ pc has a similar [Fe/H] to stars located in the central cluster at $R < 0.5$ pc. In the future, abundance measurements of CNO and α elements are planned to provide a complete view of the abundance patterns of the stars in the central regions of the Milky Way.

Support for this work was generously provided by the National Science Foundation through NSF grant AST-9619230 to K. S. and R. D. B. S. V. R. also gratefully acknowledges support from a Gemini Fellowship (grant GF-1003-97 from the Association of Universities for Research in Astronomy, Inc., under NSF cooperative agreement AST-8947990 and from Fundación Andes under project C-12984), from an Ohio State Presidential Fellowship, and from an Ohio State Alumni Research Award. S. C. B. acknowledges support from NSF grants AST-9618335 and AST-9819870, and J. S. C. from the Office of Naval Research. S. V. R. would like to thank E. Luck, R. Kraft, B. Plez, A. Pradhan, R. Pogge, A. Gould, A. Sills, and C. Sneden for useful suggestions and enlightening comments. We thank D. Figer for his generosity in sharing his spectrum of IRS 7 in advance of publication. Electronic versions of our spectra are available upon request to S. V. R.

REFERENCES

Afflerbach, A., Churchwell, E., & Werner, M. W. 1997, ApJ, 478, 190
Audouze, J., & Tinsley, B. M. 1976, ARA&A, 14, 43
Auman, J. R., & Woodrow, J. E. J. 1975, ApJ, 197, 163
Baldwin, J. R., Frogel, J. A., & Persson, S. E. 1973, ApJ, 184, 427
Blitz, L., Binney, J., Lo, K. Y., Bally, J., & Ho, P. T. P. 1993, Nature, 361, 417
Blum, R. D., Sellgren, K., & DePoy, D. D. 1996a, ApJ, 470, 864
———. 1996b, AJ, 112, 1988
Carr, J. S., Sellgren, K., & Balachandran, S. C. 2000, ApJ, 530, 307
Chiappini, C., Matteucci, F., & Padoan, P. 2000, ApJ, 528, 711
Dyck, H. M., van Belle, G. T., & Thompson, R. R. 1998, ApJ, 116, 981
Edmonds, F. N. 1969, J. Quant. Spectrosc. Radiat. Transfer, 9, 1427
Elias, J. H., Frogel, J. A., & Humphreys, R. M. 1985, ApJS, 57, 91
Fernández-Villacañas, J. L., Rego, M., & Cornide, M. 1990, AJ, 99, 1961
Fich, M., & Silkey, M. 1991, ApJ, 366, 107
Figer, D. F., Kim, S. S., Morris, M., Serabyn, E., Rich, R. M., & McLean, I. S. 1999, ApJ, 525, 750
Gray, D. F. 1992, The Observation and Analysis of Stellar Photospheres (2d ed.; Cambridge: Cambridge Univ. Press)
Gray, D. F., & Martin, B. E. 1979, ApJ, 231, 139
Güsten, R. 1989, in IAU Symp. 136, The Center of the Galaxy, ed. M. Morris (Dordrecht: Reidel), 89
Gummersbach, C. A., Kaufer, A., Schäfer, D. R., Szeifert, T., & Wolf, B. 1998, A&A, 338, 881
Holweger, H., Bard, A., Kock, A., & Kock, M. 1991, A&A, 249, 545
Jenkins, A., & Binney, J. 1994, MNRAS, 270, 703
Kleinmann, S. G. & Hall, D. N. B. 1986, ApJS, 62, 501
Kurucz, R. L. 1993, Kurucz CD-ROM 13, ATLAS9 Stellar Atmosphere Programs and the 2 km/s Grid (Cambridge: SAO)
Lambert, D. L., Brown, J. A., Hinkle, K. H., & Johnson, H. R. 1984, ApJ, 284, 223
Lang, K. R. 1991, Astrophysical Data: Planets and Stars (New York: Springer)
Livingstone, W., & Wallace, L. 1991, An Atlas of the Solar Spectrum in the Infrared from 1850 to 9000 cm^{-1} (1.1 to 5.4 μm) (NSO Tech. Report 91-001) (Tucson: National Solar Observatory)
Luck, R. E. 1982a, ApJ, 256, 177
———. 1982b, ApJ, 263, 215
Luck, R. E., & Bond, H. E. 1989, ApJS, 71, 559
Maciel, W. J., & Köppen, J. 1994, A&A, 282, 436
Marigo, P., Bressan, A., & Chiosi, C. 1996, A&A, 313, 545
McWilliam, A. 1990, ApJS, 74, 1075
McWilliam, A., & Rich, R. M. 1994, ApJS, 91, 749
Moneti, A., Glass, I. S., & Moorwood, A. F. M. 1994, MNRAS, 268, 194
Morris, M., & Serabyn, E. 1996, ARA&A, 34, 645
Najarro, F., Hillier, D. J., Figer, D. F., & Geballe, T. R. 1999, in ASP Conf. Ser. 186, The Central Parsecs of the Galaxy, ed. H. Falcke, A. Cotera, W. J. Duschl, F. Melia, & M. J. Rieke (San Francisco: ASP), 340
Nave, G., Johansson, S., Learner, R. C. M., Throne, A. P., & Brault, J. W. 1994, ApJS, 94, 221
Pagel, B. E. J., & Edmunds, M. G. 1981, ARA&A, 19, 77
Peterson, R. C., Dalle Ore, C. M., & Kurucz, R. L. 1993, ApJ, 404, 333
Plez, B. 1992, A&AS, 94, 527
Plez, B., Brett, J. M., & Nordlund, A. 1992, A&A, 256, 551
Portinari, L., & Chiosi, C. 1999, A&A, 350, 827
Rana, N. C. 1991, ARA&A, 29, 129
Reid, M. J. 1993, ARA&A, 31, 345
Richichi, A., Ragland, S., Stecklum, B., & Leinert, Ch. 1998, A&A, 338, 527
Rudolph, A. L., Simpson, J. P., Haas, M. R., Erickson, E. F., & Fich, M. 1997, ApJ, 489, 94
Ruland, F., Holweger, H., Griffin, R., & Biehl, D. 1980, A&A, 92, 70
Sadler, E. M., Rich, R. M., & Terndrup, D. M. 1996, AJ, 112, 171
Samland, M., Hensler, G., & Theis, Ch. 1997, ApJ, 476, 544
Schaerer, D., Charbonnel, C., Meynet, G., Maeder, A., & Schaller, G. 1993, A&AS, 102, 339
Schaller, G., Schaerer, D., Meynet, G., & Maeder, A. 1992, A&AS, 96, 269
Serabyn, E., & Morris, M. 1996, Nature, 382, 602
Shaver, P. A., McGee, R. X., Newton, L. M., Danks, A. C., & Pottasch, S. R. 1983, MNRAS, 204, 53
Shields, G. A. 1990, ARA&A, 28, 525
Simpson, J. P., Colgan, S. W. J., Rubin, R. H., Erickson, E. F., & Haas, M. R. 1995, ApJ, 444, 721
Smartt, S. J., & Rolleston, W. R. J. 1997, ApJ, 481, L47
Smith, V. V., & Lambert, D. L. 1985, ApJ, 294, 326
———. 1986, ApJ, 311, 843
———. 1990, ApJS, 72, 387

Sneden, C. 1973, Ph.D. thesis, Univ. of Texas
Stark, A. A., Bally, J., Gerhard, O. E., & Binney, J. 1991, MNRAS, 248, 14P
Steenbock, W. 1985, in Cool Stars with Excess of Heavy Elements, ed. M. Jaschek & P. C. Keenan (Dordrecht: Reidel), 231
Takeda, Y. 1991, A&A, 242, 455
Thévenin, F., & Idiart, T. P. 1999, ApJ, 521, 753
Tinsley, B. M., & Larson, R. B. 1978, ApJ, 221, 554
Tokunaga, A. T., Toomey, D. W., Carr, J. S., Hall, D. N. B., & Epps, H. W. 1990, Proc. SPIE, 1235, 131
Tomkin, J., & Lambert, D. L. 1983, ApJ, 273, 722
Vílchez, J. M., & Esteban, C. 1996, MNRAS, 280, 720
Wallace, L., & Hinkle, K. 1996, ApJS, 107, 312
Wheeler, J. C., Sneden, C., & Truran, J. W. 1989, ARA&A, 27, 279